

Spinteract: A Program to Refine Magnetic Interactions to Diffuse Scattering Data

Joseph A. M. Paddison*

*Materials Science and Technology Division, Oak Ridge National Laboratory, Oak Ridge, TN 37831, USA and
Churchill College, University of Cambridge, Storey's Way, Cambridge, CB3 0DS, U.K.*

Magnetic diffuse scattering—the broad magnetic scattering features observed in neutron-diffraction data above a material’s magnetic ordering temperature—provides a rich source of information about the material’s magnetic Hamiltonian. However, this information has often remained under-utilised due to a lack of available computer software that can fit values of magnetic interaction parameters to such data. Here, an open-source computer program, Spinteract, is presented, which enables straightforward refinement of magnetic interaction parameters to powder and single-crystal magnetic diffuse scattering data. The theory and implementation of this approach are summarised. Examples are presented of refinements to published experimental diffuse-scattering data sets for the canonical antiferromagnet MnO and the highly-frustrated classical spin liquid $\text{Gd}_3\text{Ga}_5\text{O}_{12}$. Guidelines for data collection and refinement are outlined, and possible developments of the approach are discussed.

I. INTRODUCTION

Magnetic materials show a wide variety of interesting and important phenomena, ranging from spin-liquid phases to multiferroicity [1–3]. A prerequisite for understanding such behaviour is often to determine the underlying magnetic interactions. The “gold standard” approach to achieve this aim typically involves performing inelastic neutron scattering experiments on a material below its magnetic ordering temperature T_N , and then fitting an interaction model to the observed spin-wave (magnon) spectra using linear spin-wave theory [4–7]. This approach was pioneered in the 1950s and 1960s, and has since been successfully applied to a wide range of materials. The recent development of powerful yet user-friendly computer software to perform spin-wave calculations, such as the SpinW code [8], has played a crucial role in popularising the application of the approach.

The spin-wave approach to determining magnetic interactions is highly successful, but nevertheless has certain limitations. First, it is often relatively time-consuming, because two different neutron-scattering experiments are typically required—diffraction measurements to determine the ordered magnetic structure of a material, followed by inelastic neutron-scattering measurements to parametrise its magnetic interactions. Second, the application of LSWT assumes a magnetic state with long-range order [4, 7]. It is therefore unsuitable for materials that do not show long-range magnetic order at experimentally-accessible temperatures, such as those with spin-liquid or spin-glass ground states [1, 2, 9]. It also requires that the magnetic structure is well understood, which may not be the case for complex phases such as non-coplanar spin textures. Third, robust fitting of magnetic interactions to measured magnon intensities is computationally expensive; this is true in particular for data collected on powder rather than single crystal samples, due to the requirement to spherically average the calculated intensities.

An alternative approach to determine magnetic interactions employs neutron-diffraction measurements performed *above*

T_N . In the paramagnetic phase, spin-pair correlations are short-ranged in real space and therefore give rise to broad scattering features, which are known as magnetic diffuse scattering. It has long been recognised that diffuse-scattering data are sensitive to the underlying magnetic interactions; e.g., in 1964, Blech and Averbach studied the magnetic diffuse scattering of the prototypical antiferromagnetic MnO above its T_N [10], and extracted an estimate of the dominant exchange interaction in good agreement with recent results [11]. Since that time, magnetic diffuse-scattering experiments have provided valuable insight into the magnetic interactions in materials such as spin ices [12–15], spin-liquid candidates [16–21], and skyrmion crystals [22, 23]. Furthermore, it was recently shown that diffuse-scattering data are also sensitive to bond-dependent magnetic interactions [24], such as those implicated in the celebrated Kitaev model [25]. In all cases, the reason for this sensitivity is that the magnetic diffuse scattering changes continuously as the interaction space is traversed. By contrast, the magnetic Bragg scattering measured below T_N provides little information about the underlying interactions, because the same ordered magnetic structure is typically obtained throughout wide regions of interaction space.

Traditionally, diffuse-scattering analysis approaches were developed specifically for the problem at hand, because general-purpose software was not available. Recently, programs to analyse magnetic diffuse-scattering data have been developed that fit local spin arrangements directly to experimental data, using either “big box” methods such as reverse Monte Carlo refinement [26–33], or “small box” methods such as magnetic pair-distribution function analysis [34–38]. These approaches aim to describe the correlations between spin pairs using methods familiar from crystal-structure refinement, and have provided important insights into the physics of disordered magnetic states, from magnetic nanoparticles [36] to emergent partial magnetic ordering [39]. However, such approaches are limited in the sense that they aim to determine only the spin correlations—not the magnetic interactions that drive them.

Here, I present a computer program, Spinteract, which calculates magnetic diffuse scattering data from interaction models and fits interaction parameter values directly to experimental data. The Spinteract program can analyse multiple

* paddisonja@ornl.gov

data sets simultaneously, including powder diffuse scattering, single-crystal diffuse scattering, and bulk magnetic susceptibility. This article is structured as follows. I begin by introducing the types of spin Hamiltonian that can be modeled using Spinteract, and the theory used to calculate the magnetic diffuse scattering from the interaction parameters. I summarise the refinement procedure in Spinteract. I benchmark the program using previously-published experimental data on two well-studied magnetic materials—the canonical antiferromagnet MnO [5, 10, 11, 32, 35] and the classical spin liquid Gd₃Ga₅O₁₂ [40–45]—and show that the analysis is consistent with published results, and also allows testing of models that extend the previous analyses. I then summarise experimental considerations that enable accurate measurement of diffuse scattering patterns, and successful refinement strategies. I conclude by discussing potential applications and developments of this approach.

II. THEORY

A. Spin Hamiltonian

Let us first introduce the types of spin Hamiltonians that are considered in Spinteract. Throughout, I consider a crystal with N magnetic atoms in its primitive unit cell; for simplicity, it is assumed that these atoms are crystallographically equivalent. A spin in the crystal is denoted $\mathbf{S}_i(\mathbf{r})$, where $i \in \{1, N\}$ labels an atomic position \mathbf{R}_i in the primitive unit cell, and \mathbf{r} is a lattice vector giving the origin of this unit cell within the crystal. The spin quantum number is S and, in the classical approximation, the spins are taken as vectors of length $\sqrt{S(S+1)}$ in the spin-only case. The g -factor is assumed to be isotropic, so that the magnetic dipole moment $\mathbf{m} = g\mathbf{S}$, but the extension to anisotropic g -factors is straightforward. Throughout, I will consider only bilinear interactions.

The spin Hamiltonian in zero applied magnetic field can be written as the sum of a single-ion term and H_{si} and a pairwise interaction term H_{ex} ,

$$H = H_{\text{si}} + H_{\text{ex}}. \quad (1)$$

In many magnetic materials, especially insulating compounds containing magnetic transition-metal ions, pairwise interactions can be approximated by the isotropic (Heisenberg) form,

$$H_{\text{ex,iso}} = -\frac{1}{2} \sum_{i,\mathbf{r}} \sum_{j,\mathbf{r}'} J_{ij}^{\text{iso}}(\mathbf{r}' - \mathbf{r}) \mathbf{S}_i(\mathbf{r}) \cdot \mathbf{S}_j(\mathbf{r}'), \quad (2)$$

where $J_{ij}^{\text{iso}}(\mathbf{r}' - \mathbf{r})$ is the Heisenberg interaction parameter for the bond connecting site i in primitive cell \mathbf{r} with site j in primitive cell \mathbf{r}' . Usually, these interaction are restricted to near-neighbour distances, such that $J_{ij}(\mathbf{r}' - \mathbf{r}) \in \{J_1, J_2, \dots, J_n\}$, where J_n denotes an interaction between n -th nearest neighbours. Spinteract uses the convention that ferromagnetic interactions correspond to positive values of J , and each pair of spins is counted once in the double summation.

The Heisenberg form can be generalised to include anisotropic interactions,

$$H_{\text{ex}} = -\frac{1}{2} \sum_{i,\mathbf{r}} \sum_{j,\mathbf{r}'} \sum_{\alpha,\beta} J_{ij}^{\alpha\beta}(\mathbf{r}' - \mathbf{r}) S_i^\alpha(\mathbf{r}) S_j^\beta(\mathbf{r}'), \quad (3)$$

where $\alpha, \beta \in x, y, z$ denote spin components with respect to a set of local principal axes (discussed below). This can include, for example, the XXZ model ($J^{xx} = J^{yy} \neq J^{zz}$) as well as interactions that depend on the orientations of bonds connecting spin pairs, such as the Kitaev interaction [25].

A special case is the long-ranged magnetic dipolar interaction, given by

$$H_{\text{dip}} = \frac{g^2 D_{\text{dip}} |\mathbf{r}_{\text{nn}}|^3}{2} \sum_{i,\mathbf{r}} \sum_{j,\mathbf{r}'} \frac{\{\mathbf{S}_i(\mathbf{r}) \cdot \mathbf{S}_j(\mathbf{r}') - 3[\mathbf{S}_i(\mathbf{r}) \cdot \hat{\mathbf{r}}_{ij}][\mathbf{S}_j(\mathbf{r}') \cdot \hat{\mathbf{r}}_{ij}]\}}{|\mathbf{r}_{ij}|^3}, \quad (4)$$

where $\hat{\mathbf{r}}_{ij}$ is a unit vector parallel to the vector connecting spin pairs in the crystal, and $D_{\text{dip}} = \mu_0 \mu_B^2 / 4\pi k_B |\mathbf{r}_{\text{nn}}|^3$ is the magnitude of the dipolar interaction at the nearest-neighbour distance, $|\mathbf{r}_{\text{nn}}|$. The magnetic dipolar interaction is usually negligible compared to the exchange interaction in transition-metal compounds, but can be significant in rare-earth compounds, where exchange interactions are often weak but magnetic moments can have large magnitudes. In Spinteract, the magnetic dipolar interaction is implemented using Ewald summation, as described in Ref. [46].

The form of the single-ion Hamiltonian H_{si} depends on the point symmetry of the magnetic site. For cubic site symmetries, no bilinear single-ion term is allowed. For lower site symmetries, the single-ion Hamiltonian is given by

$$H_{\text{si}} = -D \sum_{i,\mathbf{r}} [S_i^z(\mathbf{r})]^2 - E \sum_{i,\mathbf{r}} \{[S_i^x(\mathbf{r})]^2 - [S_i^y(\mathbf{r})]^2\}, \quad (5)$$

where positive values of D imply easy-axis anisotropy, and negative values of D imply easy-plane anisotropy. Axial site symmetries (hexagonal, trigonal, or tetragonal) allow only $D \neq 0$, whereas rhombic site symmetries (orthorhombic, monoclinic, and triclinic) allow both $D \neq 0$ and $E \neq 0$. In Eq. (5), x , y and z denote spin components with respect to mutually-orthogonal principal axes, $\hat{\mathbf{n}}^x, \hat{\mathbf{n}}^y, \hat{\mathbf{n}}^z$, which are ‘‘local’’ as they can be different for each magnetic site in the unit cell. In axial site symmetries, one of the principal axes (conventionally $\hat{\mathbf{n}}^z$) is aligned with the high-symmetry local rotation axis, and the remaining two axes are mutually orthogonal in the perpendicular plane. In orthorhombic point groups, the principal axes are parallel to the three two-fold rotation axes. In monoclinic point groups, one axis is parallel to the two-fold rotation axis. Additional measurements, such as bulk susceptibility or spherical neutron polarimetry [47], are needed to indicate an appropriate axis within the perpendicular plane. Once the local axes have been defined for one atomic position in the unit cell, they can be generated for all others by applying space-group symmetry operations.

The dimensionality n of the spins may be effectively reduced in the limit of strong axial anisotropy, which occurs when $|D| \gg k_B T$. Then, instead of considering Heisenberg spins ($n = 3$), we may consider Ising spins ($n = 1$) for strong

easy-axis anisotropy, or XY spins ($n = 2$) for strong easy-plane anisotropy.

B. Magnetic neutron scattering intensity

Our goal here is to express the diffuse magnetic neutron-scattering intensity for $T > T_N$ in terms of the underlying magnetic interactions. This requires either analytical approximations, such as field theories, or numerical simulations, such as Monte Carlo simulations. Spinteract uses a self-consistent extension of mean-field theory called Onsager reaction-field theory [48–53]. This approach takes account of thermal fluctuations in an approximate way, but has been shown to give results in excellent agreement with Monte Carlo simulations [24, 54]. The equations underlying this approach are discussed in the literature for special cases [24, 48–51]; I sketch the derivation of the general case below. The key results are given in Eqs. (17)–(19).

I start with the general expression for the energy-integrated magnetic neutron-scattering intensity from spin-only moments a single crystal [55],

$$I(\mathbf{Q}) = \frac{C[gf(Q)]^2}{N} \sum_{i,j} \langle \mathbf{S}_i^\perp(-\mathbf{Q}) \cdot \mathbf{S}_j^\perp(\mathbf{Q}) \rangle \exp[i\mathbf{Q} \cdot (\mathbf{R}_j - \mathbf{R}_i)], \quad (6)$$

where $f(Q) = f(|\mathbf{Q}|)$ is the magnetic form factor [56], and

$$\mathbf{S}_i^\perp = \mathbf{S}_i - \mathbf{Q} \mathbf{S}_i \cdot \mathbf{Q} / Q^2 \quad (7)$$

is the projection of the spin perpendicular to \mathbf{Q} . The Fourier transform of a spin component is defined by

$$S_i^\alpha(\mathbf{Q}) = \sum_{\mathbf{r}} S_i^\alpha(\mathbf{r}) \exp(i\mathbf{Q} \cdot \mathbf{r}) \quad (8)$$

and the Fourier transform of the exchange interaction is defined by

$$J_{ij}^{\alpha\beta}(\mathbf{Q}) = \sum_{\mathbf{r}'-\mathbf{r}} J_{ij}^{\alpha\beta}(\mathbf{r}'-\mathbf{r}) \exp[-i\mathbf{Q} \cdot (\mathbf{r}'-\mathbf{r})], \quad (9)$$

which is independent of the choice of the unit cell \mathbf{r} at the origin. The $J_{ij}^{\alpha\beta}$ describe a $nN \times nN$ Hermitian “interaction matrix” at each wavevector, where n is the spin dimension.

The Onsager reaction-field approach consider the spin alignment induced by a site-dependent applied field $H_i^\alpha(\mathbf{Q})$, which leads to an effective field at site i given by

$$H_{i,\text{eff}}^\alpha(\mathbf{Q}) = H_i^\alpha(\mathbf{Q}) - \lambda S_i^\alpha(\mathbf{Q}) + \sum_j J_{ij}^{\alpha\beta}(\mathbf{Q}) S_j^\beta(\mathbf{Q}). \quad (10)$$

Here, λ is the reaction field, which is a temperature-dependent parameter that is subtracted from the mean field to account for the effect of local spin correlations. It is determined at each temperature by enforcing the self-consistency condition on the average spin length,

$$\frac{1}{NN_{\mathbf{q}}} \sum_{\alpha,i,\mathbf{q}} \langle S_i^\alpha(\mathbf{q}) S_i^\alpha(-\mathbf{q}) \rangle = S(S+1), \quad (11)$$

where the sum is taken over $N_{\mathbf{q}}$ wavevectors \mathbf{q} in the first Brillouin zone [48–51]. The mean-field approximation corresponds to $\lambda = 0$ at all temperatures.

The calculation proceeds by writing the spin in terms of normal-mode variables that are indexed by $\mu \in \{1, nN\}$,

$$S_i^\alpha(\mathbf{Q}) = \sum_{\mu} S_{\mu}(\mathbf{Q}) U_{i\mu}^\alpha(\mathbf{Q}), \quad (12)$$

where S_{μ} is the amplitude of mode μ . An analogous decomposition is made for the field $H_i^\alpha(\mathbf{Q})$. The interaction matrix is diagonalised by transforming it to normal-mode variables,

$$\lambda_{\mu}(\mathbf{Q}) U_{i\mu}^\alpha(\mathbf{Q}) = \sum_j J_{ij}^{\alpha\beta}(\mathbf{Q}) U_{j\mu}^\beta(\mathbf{Q}), \quad (13)$$

where $\lambda_{\mu}(\mathbf{Q})$ are eigenvalues of the interaction matrix, and the eigenvector components $U_{i\mu}^\alpha(\mathbf{Q})$ are normalised such that $\sum_{i,\alpha} U_{i\mu}^\alpha(\mathbf{Q}) U_{i\nu}^\alpha(-\mathbf{Q}) = \delta_{\mu\nu}$. These eigenvalues and eigenvectors contain important information about the physics of the system. In particular, for a given set of interaction parameters, the wavevector at which the global maximum eigenvalue λ_{max} occurs is the propagation vector of the magnetically-ordered state that develops at T_N . In the absence of frustration, λ_{max} occurs at a small number of wavevectors related by symmetry. In highly-frustrated systems, by contrast, there is a large degeneracy of wavevectors with maximum eigenvalues close to λ_{max} [57, 58].

Using the definition of the single-ion (Curie) susceptibility,

$$\chi_0 = \frac{S(S+1)}{nT}, \quad (14)$$

and Eqs. (8)–(9) and (12)–(14) in Eq. (10), we obtain the wavevector-dependent magnetic susceptibility $\chi_{\mu}(\mathbf{Q}) = S_{\mu}(\mathbf{Q})/H_{\mu}(\mathbf{Q})$ for each normal mode,

$$\chi_{\mu}(\mathbf{Q}) = \frac{\chi_0}{1 - \chi_0 [\lambda_{\mu}(\mathbf{Q}) - \lambda]}. \quad (15)$$

The magnetic ordering temperature T_N of the model is the highest temperature at which the denominator of Eq. (15) is equal to zero, for any wavevector and any mode. The wavevector-dependent susceptibility is closely related to the correlation function of mode amplitudes, *via* the high-temperature limit of the fluctuation-dissipation theorem [55],

$$\chi_{\mu}(\mathbf{Q}) = \frac{1}{T} \langle S_{\mu}(\mathbf{Q}) S_{\mu}(-\mathbf{Q}) \rangle. \quad (16)$$

The final result for the diffuse scattering intensity is obtained by using Eqs. (12), (15), and (16) in Eq. (6):

$$I(\mathbf{Q}) = \frac{C[\mu f(Q)]^2}{N} \sum_{\mu=1}^{nN} \frac{|\mathbf{s}_{\mu}^\perp(\mathbf{Q})|^2}{1 - \chi_0 [\lambda_{\mu}(\mathbf{Q}) - \lambda]}, \quad (17)$$

in which

$$\mathbf{s}_{\mu}^\perp(\mathbf{Q}) = \sum_{i,\alpha} (\hat{\mathbf{n}}_i^\alpha - \mathbf{Q} \hat{\mathbf{n}}_i^\alpha \cdot \mathbf{Q} / Q^2) U_{i\mu}^\alpha(\mathbf{Q}) \exp(i\mathbf{Q} \cdot \mathbf{R}_i) \quad (18)$$

and the magnetic moment $\mu = g\sqrt{S(S+1)}$. The reaction field is determined at each temperature by requiring that

$$\sum_{\mu, \mathbf{q}} [1 - \chi_0(\lambda_\mu(\mathbf{q}) - \lambda)]^{-1} = nNN_{\mathbf{q}}, \quad (19)$$

which follows from Eq. (11), (12), (15), and (16).

The first term in brackets in Eq. (18) accounts for the fact that neutrons are only sensitive to magnetisation components perpendicular to \mathbf{Q} . This direction dependence allows magnetic diffuse scattering measurements to be sensitive to the bond-dependence of interactions, enabling investigation of non-Heisenberg interactions [24]. In the limit of Heisenberg spins with entirely isotropic interactions, only one spin component needs to be considered, and Eq. (17) simplifies to

$$I_{\text{iso}}(\mathbf{Q}) = \frac{2C[\mu f(Q)]^2}{3N} \sum_{\mu=1}^N \frac{|\sum_i U_{i\mu}(\mathbf{Q}) \exp(i\mathbf{Q} \cdot \mathbf{R}_i)|^2}{1 - \chi_0[\lambda_\mu(\mathbf{Q}) - \lambda]}. \quad (20)$$

Finally, to compare calculations with data collected on powder samples, it is necessary to perform a spherical average of Eq. (17) to obtain $I(Q)$. In Spinteract, the spherical average is performed numerically using the method of Lebedev quadrature [59]. This approach is advantageous because the distribution of samples has $m\bar{3}m$ Laue symmetry, which allows a large reduction in the number of wavevectors that must be sampled in high-symmetry systems.

C. Magnetic susceptibility

The bulk magnetic susceptibility χ for a powder sample is obtained from

$$\chi T = \frac{\mu^2}{nN} \sum_{\mu=1}^{nN} \frac{|\sum_{i,\alpha} \hat{\mathbf{n}}_i^\alpha U_{i\mu}^\alpha(\mathbf{0})|^2}{1 - \chi_0[\lambda_\mu(\mathbf{0}) - \lambda]} \quad (21)$$

in the general case, and

$$\chi_{\text{iso}} T = \frac{\mu^2}{N} \sum_{\mu=1}^N \frac{|\sum_i U_{i\mu}(\mathbf{0})|^2}{1 - \chi_0[\lambda_\mu(\mathbf{0}) - \lambda]} \quad (22)$$

in the isotropic case. Since the bulk magnetic susceptibility measures $\mathbf{Q} = \mathbf{0}$, only the normal mode corresponding to ferromagnetic spin alignment contributes to it. The eigenvalue for this mode

$$\begin{aligned} \lambda_{\text{bulk}} &= \sum_n J_n Z_n \\ &= 3\theta_W / S(S+1), \end{aligned}$$

where Z_n is the coordination number for n -th neighbour interactions, and θ_W is the Weiss temperature that is commonly fitted to bulk magnetic susceptibility data at high temperatures [60]. Note that Eq. (22) reproduces the Curie-Weiss law in the mean-field approximation ($\lambda = 0$).

D. Advantages and limitations

The reaction-field approach described has two key properties that make it useful for fitting magnetic diffuse scattering data. First, each scattering calculation is relatively fast, typically taking no more than a few seconds. Second, unlike statistical approaches such as Monte Carlo simulations, the calculation results do not contain statistical noise. This is important because most fitting algorithms numerically calculate derivatives of the goodness-of-fit metric as a key step, which requires that the calculated curves are free from noise.

Onsager reaction-field theory, and an equivalent theory called the self-consistent Gaussian approximation (SCGA) [54, 61], have been shown to give accurate results for realistic magnetic models. For example, a study of the frustrated Heisenberg model on the pyrochlore lattice considered antiferromagnetic nearest-neighbour interactions and various further neighbor interactions, and found that the scattering patterns obtained from the SCGA were in excellent agreement with Monte Carlo simulations over a wide temperature range [54]. Subsequently, reaction-field calculations involving bond-dependent interactions on triangular and honeycomb lattices were compared with Monte Carlo simulation results, again showing good agreement between the two approaches [24]. These comparisons allow confidence in applying the approach to materials where the Hamiltonian is not yet known.

The reaction-field approach also has some limitations. It is only exact for classical spins in the high-temperature limit, and becomes less accurate close to a magnetic ordering transition, although it is notable that a reaction-field study of MnO obtained results for $T \gtrsim T_N$ that were comparable to those at higher temperatures [11]. Importantly, reaction-field calculations are much less accurate for systems with low coordination numbers, such as quasi-one-dimensional magnets [53, 62], and Spinteract should be used with caution in such systems. Reaction-field theory also does not consider effects arising from quantum fluctuations, order-by-disorder, or partial magnetic ordering where magnetic Bragg and diffuse scattering coexist.

III. IMPLEMENTATION

In Spinteract, interaction parameters can be fitted to multiple data sets simultaneously, including powder and single-crystal magnetic diffuse-scattering data, and powder bulk magnetic susceptibility. The user provides a keyword-based text file containing crystallographic information (unit-cell parameters and fractional coordinates of magnetic atoms) and magnetic information (spin dimensionality n , spin magnitude, magnetic form factor, and local principal axes, if required). The user also specifies the interaction parameters included in the model and their initial values. Spinteract can automatically implement Heisenberg interactions J_{iso} for arbitrary neighbours, anisotropic interactions J_{xx} , J_{yy} , and J_{zz} , the long-ranged dipolar interaction D_{dip} , and single-ion anisotropy terms D and E . If more complex interactions are required, custom coupling matrices can be de-

fined. Detailed instructions are provided with Spinteract, which is open-source software and may be downloaded from www.joepaddison.com/software.

Spinteract comprises a Fortran subroutine that calculates the sum of squared residuals, defined as

$$\chi^2 = \sum_d W_d \sum_{i \in d} \left(\frac{I_i^{\text{data}} - s_d I_i^{\text{calc}}}{\sigma_i} \right)^2, \quad (23)$$

where d denotes a data set with weight W_d , I_i^{data} is the intensity of data point i , I_i^{calc} is the calculated intensity obtained from Eqs. (17)–(20), σ_i is the corresponding uncertainty, and s_d is an (optional) refined intensity scale factor which is determined for each dataset from the linear-least-squares relation [63]

$$s_d = \frac{\sum_i I_i^{\text{data}} I_i^{\text{calc}} / \sigma_i^2}{\sum_i (I_i^{\text{calc}})^2 / \sigma_i^2}. \quad (24)$$

This is necessary because neutron-scattering data are typically not placed in absolute intensity units of $\text{bn sr}^{-1} \text{spin}^{-1}$. In Spinteract, this equation can be extended so that an intensity offset is also refined [63], to account for residual background scattering or incoherent scattering. These profile parameters can be constrained to be the same for all datasets, if needed.

The fitting procedure—the minimisation of Eq. (23) by varying the interaction parameters—is performed using the well-established program Minuit [64, 65]. All the capabilities of Minuit, such as estimation of parameter uncertainties and contour plotting of χ^2 , are accessible in Spinteract. Minuit includes several different fitting algorithms, but the most widely used is the Migrad algorithm, which implements a variant of the Davidon-Fletcher-Powell algorithm for non-linear least squares fitting. This algorithm was used for the examples discussed in the following section.

A Spinteract calculation proceeds as follows. First, if a centred unit cell is specified, the unit cell is transformed to the primitive setting, to enable calculation of the interaction matrices in their most compact form. Second, the interaction matrix is calculated from Eq. (9) for the current interaction parameters, and diagonalised on a grid in the primitive cell in reciprocal space (equivalent to the first Brillouin zone). Third, the reaction field is calculated at each temperature *via* Eq. (19). Fourth, the scattering intensity is calculated *via* Eqs. (17)–(20), and spherically averaged if needed. Fifth, the goodness-of-fit metric χ^2 is obtained from Eq. (23), and the optimal intensity scale and background factors are determined. If the interactions are being refined, χ^2 for the current interaction parameters is sent to the Minuit fitting program, and Minuit returns a new set of interactions for the next iteration of the fit.

After the fit has converged, Spinteract outputs the calculated scattering patterns for the optimised parameter values. Spinteract also outputs a summary of the model parameter values, uncertainties, and refinement metrics in LaTeX format, for straightforward integration into future publications.

IV. EXAMPLES

In this section, I present examples of Spinteract refinements to experimental neutron-scattering data for two well-studied materials: the canonical antiferromagnet MnO and the well-known frustrated magnet $\text{Gd}_3\text{Ga}_5\text{O}_{12}$. These examples are not intended primarily to uncover new information about these materials, but rather as test cases that demonstrate the effectiveness of the approach. However, we will see that these refinements allow some new information to be determined.

A. Single crystal data: MnO

Manganese(II) oxide, MnO, plays a central role in the history of neutron scattering—it was the first material in which antiferromagnetic Bragg peaks were observed below its T_N of 118 K, providing the first direct experimental evidence for antiferromagnetism [66]. In the 1960s, magnetic diffuse scattering was reported above T_N . An early powder diffuse-scattering analysis identified that the dominant magnetic interactions between $S = 5/2$ magnetic moments of Mn^{2+} was the next-nearest neighbour Heisenberg term, which was estimated to have an antiferromagnetic value of $J_2 = 4.65 \text{ meV}$ [10]. Subsequently, an analysis of single-crystal diffuse scattering obtained antiferromagnetic $J_1 = 3.31 \text{ K}$ and $J_2 = 4.69 \text{ K}$ at $T \approx 160 \text{ K}$ using the Onsager reaction-field approach [11], which showed reasonable consistency with values extrapolated from low-temperature spin-wave-dispersion measurements [5]. MnO has also been investigated by reverse Monte Carlo analysis of powder [27] and single-crystal [32] samples, as well as by magnetic pair-distribution-function analysis of powder samples [35], which confirm that antiferromagnetic correlations and domain structure persist to temperatures far above T_N .

Using the Spinteract program, refinements of J_1 and J_2 were performed against experimental magnetic diffuse scattering data on MnO. The data were previously published in Ref. [32]; they were collected at $T = 160 \text{ K}$ using the SXD diffractometer at the ISIS Neutron and Muon Source, and comprise a large volume of reciprocal space ($\sim 3 \times 10^6$ data points), as shown in Fig. 1. Nuclear Bragg peaks were excluded and a measurement of an empty sample holder was subtracted from the data. Spinteract refinements of J_1 and J_2 to the entire volume of data were performed. An overall intensity scale factor and a constant-in- Q offset were also refined; the latter was needed to account for significant incoherent scattering from Mn. Despite the large number of data points, convergence was obtained after a CPU time of approximately 10 minutes on a 2.9 GHz Intel Core i5 processor. As shown in Fig. 1, an excellent fit was obtained with the refined values of J_1 and J_2 given in Table I; these values show excellent agreement (within a few per cent) with the results of Ref. [11]. Since statistical uncertainties were not reported in the original data set, parameter uncertainties could not readily be estimated. However, a further refinement in which a linear-in- Q intensity offset was also refined yielded essentially equivalent parameter values [Table I], suggesting that the results are likely to be

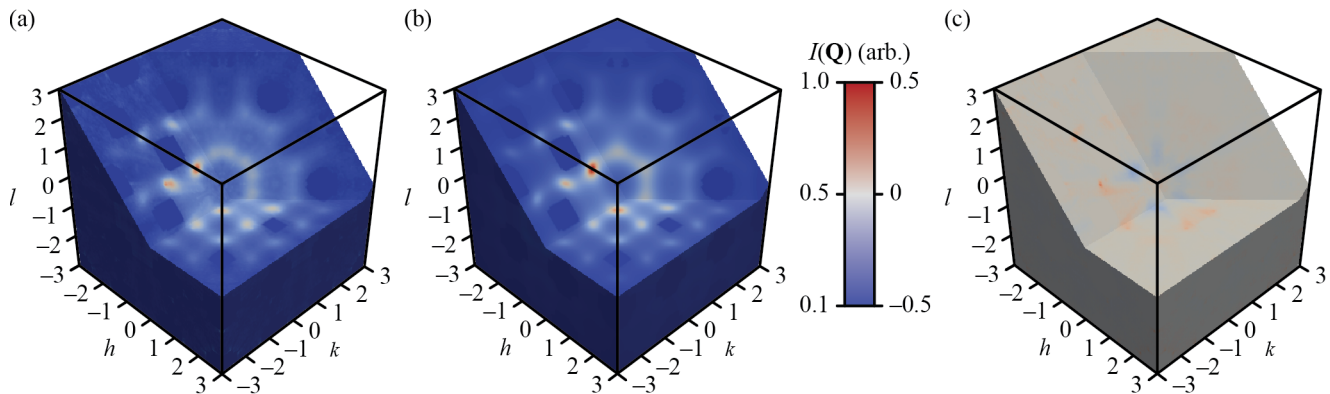


Figure 1. Single-crystal diffuse magnetic scattering for MnO, showing (a) experimental data measured at 160 K (reproduced from Ref. [32]); (b) fit obtained using Spinteract; (c) data-fit.

MnO	J_1 (K)	J_2 (K)	J_3 (K)	R_{wp}
160 K (constant offset)	3.26	4.45	0*	8.76
160 K (constant offset)	3.44	4.48	0.09	8.76
160 K (constant + Q -linear offset)	3.33	4.51	0*	8.75
160 \pm 20 K (Ref. [11])	3.31	4.59	0*	—

Table I. Values of interaction parameters for MnO, obtained from refinements to single-crystal diffuse scattering data shown in Figure 1, compared with values obtained in Ref. [11]. Interaction parameters are given for spins of magnitude $\sqrt{S(S+1)}$ with $S = 5/2$, and in the same Hamiltonian convention as previous studies, where antiferromagnetic interactions are positive and spin pairs are double counted. In the Spinteract convention defined by Eq. (2), the interaction parameters in this table would be multiplied by -2 .

robust.

A natural question is whether the magnetic interactions in MnO might extend beyond next-nearest-neighbours. To investigate this question, a further refinement was performed, in which J_3 was allowed to vary in addition to J_1 and J_2 . The refined value of J_3 is only 2% of J_2 [Table I], suggesting that interactions beyond next-nearest neighbours are indeed very weak in MnO.

B. Powder data: $\text{Gd}_3\text{Ga}_5\text{O}_{12}$

Garnet-structured $\text{Gd}_3\text{Ga}_5\text{O}_{12}$ (gadolinium gallium garnet, GGG) is a geometrically-frustrated system in which Gd^{3+} moments with $S = 7/2$ occupy two interpenetrating networks of corner-sharing triangles connected in three dimensions. It shows an unusual spin-freezing transition below $T_f \approx 0.14$ K [41], and the emergence of effective magnetic multipoles from strongly-correlated 10-spin loops above T_f [44]. Its magnetic interactions consist of the long-ranged magnetic dipolar interaction, with magnitude $D_{\text{dip}} = 0.0457$ K at the nearest-neighbour distance, and local exchange interactions extending at least to third-nearest neighbours [40, 43, 45]. The val-

ues of the exchange interactions were first investigated using a high-temperature analysis, which obtained antiferromagnetic $J_1 = 0.107$ K, $-0.015 \leq J_2 \leq 0.009$ K, and $-0.03 \leq J_3 \leq 0.100$ K [40]. A later study of magnetic critical scattering considered the incipient ordering wavevector within the spin-frozen regime, and obtained $-0.012 \leq J_2 \leq -0.004$ K and $-0.003 \leq J_3 \leq 0.012$ K [43]. A spin-wave measurement in applied magnetic field was consistent with $J_3 \approx 0.013$ K and insensitive to J_2 [45].

Spinteract refinements were performed to published powder neutron-scattering data collected over a wide temperature range above T_f , as shown in Fig. 2. These data were originally published in Ref. [42]. Initially, J_1 was kept fixed at the value of 0.107 K [40, 43] and J_2 and J_3 were refined, as in Ref. [43]. The refined fit parameters are given in Table II; they are close to the possible range reported in Ref. [43], with J_2 at the upper limit of this range and J_3 close to its lower limit. However, within this range, optimal values of $J_2 \approx -0.005$ K and $J_3 \approx 0.010$ K were also reported in Ref. [43]; the latter value is significantly different to the value from Spinteract refinement. This difference is mainly because reaction-field theory predicts an onset of long-range magnetic ordering at $T > 0.2$ K for the optimal parameter set of Ref. [43], which is inconsistent with the observation of diffuse magnetic scattering below this temperature. An extended model was therefore tested using Spinteract, where J_1 , J_2 , J_3 and J_4 were allowed to vary. This refinement yielded a significant improvement in fit quality [Fig. 2] and an antiferromagnetic value of J_3 . However, the refined value of J_4 is also significant, suggesting the possibility that interactions may extend beyond third-nearest neighbours in $\text{Gd}_3\text{Ga}_5\text{O}_{12}$.

V. GUIDANCE

The Spinteract code has already been used in several published studies [23, 24, 67, 68], allowing it to be tested on a variety of problems. Some general strategies for data collection, processing, and refinement are summarised below.

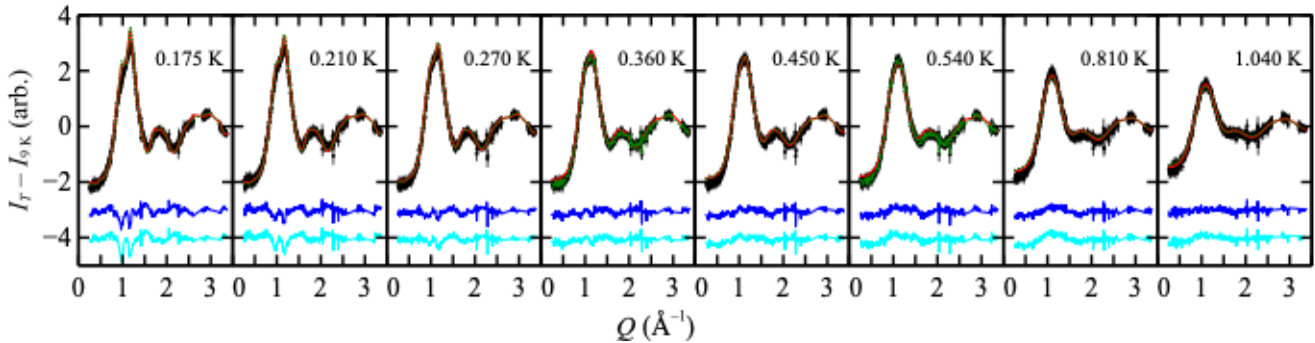


Figure 2. Powder diffuse magnetic scattering for $\text{Gd}_3\text{Ga}_5\text{O}_{12}$ at temperatures labelled in each panel. Experimental data (black circles) are reproduced from Refs. [42, 44]. Spinteract fits with variable J_1 , J_2 , J_3 , and J_4 are shown as red lines, and the corresponding difference curves (data–fit) are shown as blue lines that are vertically shifted by 3 units. Spinteract fits with variable J_2 and J_3 and fixed $J_1 = 0.107$ K and $J_4 = 0$ are shown as dotted green lines, and the corresponding difference curves (data–fit) are shown as cyan lines that are vertically shifted by 4 units.

$\text{Gd}_3\text{Ga}_5\text{O}_{12}$	J_1 (K)	J_2 (K)	J_3 (K)	J_4 (K)	R_{wp}
Fit J_2, J_3	0.107*	−0.0035(2)	−0.0015(7)	0*	13.28
Fit J_1 – J_4	0.130(2)	−0.0038(1)	0.0040(6)	0.0040(3)	12.62
Ref. [43]	0.107*	−0.012 : −0.004	−0.003 : 0.012	0*	–

Table II. Values of interaction parameters for $\text{Gd}_3\text{Ga}_5\text{O}_{12}$, obtained from refinements to powder diffuse-scattering data shown in Figure 1, compared with range of possible values obtained in Ref. [43]. In all cases, $D_{\text{dip}} = 0.0457$ K is fixed. Interaction parameters are given for spins of magnitude $\sqrt{S(S+1)}$ with $S = 7/2$, and in the same Hamiltonian convention as previous studies [40, 43], where antiferromagnetic interactions are positive and spin pairs are single counted. For the Spinteract convention defined by Eq. (2), the interaction parameters in this table would be multiplied by -1 .

A. Data collection

A key advantage of magnetic diffuse scattering is that it can often be collected using the same experimental setup as for conventional Bragg diffraction measurements, by increasing the sample temperature above T_N . Standard data corrections are required, such as for detector efficiency and absorption by the sample. For quantitative analysis of magnetic diffuse scattering data, several other considerations can be relevant:

- *Sample size, counting time, and choice of instrument.* Since diffuse scattering intensity is distributed throughout reciprocal space, the scattering intensity at any given position is typically weak. Hence, larger sample sizes and counting times may be required compared to conventional Bragg diffraction measurements. For single-crystal measurements, instruments capable of measuring a wide range of reciprocal space are usually most suitable.
- *Energy integration.* Spinteract assumes that the neutron-diffraction data are energy-integrated over the entire spin-fluctuation spectrum. This requirement is met in diffraction experiments provided that the energy change of the scattered neutrons is much smaller

than the incident neutron energy, E_i (“quasistatic approximation”). As a rule of thumb, one should choose $E_i > k_B \theta_W$, where the Weiss temperature θ_W provides an estimate of the strength of the magnetic interactions.

- *Choice of measurement temperatures.* Measuring the diffuse scattering at several temperatures above T_N provides is often helpful to determine the values of magnetic interactions, especially for complex model Hamiltonians such as those considered in Refs. [23, 24, 67, 68].

B. Data processing

Spinteract assumes that the input data contains *only* magnetic diffuse scattering. Therefore, other signals—such as nuclear Bragg scattering, incoherent scattering, and background scattering—should be removed before attempting a refinement.

- *Background subtraction.* It is important to correct diffuse-scattering data for background scattering, which could otherwise bias the fit results. This can be achieved by subtracting a measurement of the empty sample container from the sample measurement. Alternatively, the sample may be measured at a high temperature at which the spins are essentially uncorrelated, and this measurement subtracted from the data of interest. Since temperature-subtracted data reflect only a difference in spin correlation between the higher and lower temperature, this approach involves some information loss, but it is often effective in practice.
- *Removal of nonmagnetic scattering.* It is necessary to remove nonmagnetic scattering (e.g., nuclear Bragg peaks) from the data before modelling them using Spinteract. This can be achieved experimentally by performing polarisation analysis. Alternatively, unpolarised data may be post-processed, either by subtracting a high-temperature data set from the data of interest, by

excluding regions of the data containing Bragg peaks, or by performing a refinement to the nuclear Bragg profile and subtracting the fitted Bragg profile from the experimental data.

C. Data refinement

The fitting program (Minuit) used in Spinteract is highly robust; however, like any such algorithm, it can converge to a local minimum in the goodness-of-fit, or fail to converge at all. This problem is more likely to occur if the initial parameter values are too far from the optimal ones, or if the parameter values are under-constrained by the data. Some straightforward checks can help determine if the optimal solution was found:

- *Multiple refinements.* It is useful to perform multiple (e.g., 10 to 100) refinements, with different starting values of the interaction parameters. This approach often allows false (local) minima to be identified; such false minima can be neglected provided they yield much worse fits than the optimal solution.
- *Covariance matrix.* A second useful check is to examine the covariance matrix that is output by Minuit. If two (or more) parameters have a large covariance, their values may not be well determined, and it is worthwhile to check the fit dependence on these parameters using a contour plot of χ^2 .
- *Physical predictions.* Spinteract provides an estimate of T_N of the system, and the magnetic propagation vector of the ordered state that develops below T_N , based on the refined interaction model. For materials that exhibit long-range magnetic ordering, these predictions can be compared with experimental results, providing an independent check on the validity of the refined model.
- A final check on the model validity is to repeat the refinement under slightly different conditions—e.g., changing the relative weighting of susceptibility vs. diffuse-scattering data, or by allowing an extra background parameter to refine. This can provide some insight into the variation of parameter values due to systematic errors, which are often more difficult to characterise than statistical uncertainties.

If these checks suggest that the results are not well constrained by the data, the user has two options—either fix some parameters, or include more experimental data. A particularly useful approach is to fit to bulk magnetic susceptibility data as well as magnetic diffuse scattering, as in Refs. [18, 23, 68]. The magnetic susceptibility expressed as χT effectively measures the $Q \rightarrow 0$ limit of the magnetic diffuse scattering, and provides a strong constraint on the net value of the magnetic interactions (i.e., the Weiss temperature). Including the susceptibility data with a sufficiently high weight can therefore help the refinement avoid unphysical regions of parameter space.

VI. CONCLUSIONS AND OUTLOOK

The key result of this work is to provide a user-friendly computer program, Spinteract, for refinement of magnetic interactions against magnetic-diffuse scattering data. The Spinteract program allows straightforward estimation of interaction parameters from data collected in neutron-diffraction experiments. This approach has potential to accelerate the experimental determination of magnetic interaction in new materials, particularly those which cannot be prepared as large single crystals suitable for inelastic scattering measurements. Moreover, diffuse-scattering analysis can offer advantages over conventional spin-wave analysis in topical systems, such as those with spin-liquid or spin-glass ground states, or materials where a strong Ising-like magnetic anisotropy generates essentially non-dispersive spin-wave excitations [69].

The capabilities of Spinteract could be developed in several directions. First, the equations outlined in Section II assume that magnetic spins transform as dipoles. This is the most common case, and leads to a Curie-law form of the single-ion susceptibility. However, spin-orbit coupling and crystal-field effects may lead to interactions between multipolar degrees of freedom [70]. A simple example is a system in which the crystal field ground state is two singlets, separated by an energy gap Δ , in which dipolar order only develops if $J \gtrsim \Delta$ and the transverse pseudo-spin components transform as quadrupoles [71]. Such materials can be modelled within the reaction-field framework by modifying the single-ion susceptibility [72].

A second outstanding question is the extent to which this approach is applicable for correlated quantum systems, such as quantum spin-liquid candidates with effective spin- $\frac{1}{2}$. Even though the Onsager reaction-field method is semiclassical, it does not necessarily fail to describe the magnetic diffuse scattering of such systems, because thermal fluctuations dominate quantum fluctuations at sufficiently high temperature. In this way, refinements to diffuse-scattering data at high temperature may provide information about the interactions responsible for driving the system to a quantum ground state. Recently, this approach was tested in the delafossite system KYbSe_2 , where Yb^{3+} magnetic moments with effective spin- $\frac{1}{2}$ occupy a triangular lattice [73, 74]. Refinements to magnetic diffuse-scattering data at $T \geq 1$ K using the reaction-field approach yielded a ratio J_1/J_2 that is in good agreement with advanced quantum calculations [74], suggesting this approach deserves further investigation.

ACKNOWLEDGEMENTS

I am grateful to Oleg Petrenko (Warwick) and Matthias Gutmann (ISIS) for allowing re-use of their published diffuse-scattering data, and to Xiaojian Bai (Louisiana State), Stuart Calder (ORNL), Andrew Christianson (ORNL), Matthew Cliffe (Nottingham), Ovidiu Garlea (ORNL), Andrew Goodwin (Oxford), Martin Mourigal (Georgia Tech), Ross Stewart (ISIS), and Matthew Tucker (ORNL) for valuable discussions. Development of the Spinteract program was supported by a Junior Research Fellowship from Churchill College, Uni-

versity of Cambridge (U.K.) from 2016–2019. Manuscript preparation was supported by the U.S. Department of Energy,

Office of Science, Basic Energy Sciences, Materials Sciences and Engineering Division.

-
- [1] C. Broholm, *et al.*, *Science* **367** (2020).
- [2] L. Balents, *Nature* **464**, 199 (2010).
- [3] S.-W. Cheong, M. Mostovoy, *Nat. Mater.* **6**, 13 (2007).
- [4] R. Kubo, *Phys. Rev.* **87**, 568 (1952).
- [5] G. Pepy, *J. Phys. Chem. Solids* **35**, 433 (1974).
- [6] A. J. Princep, *et al.*, *npj Quantum Materials* **2**, 63 (2017).
- [7] R. S. Fishman, J. A. Fernandez-Baca, T. Rößler, *Spin-Wave Theory and its Applications to Neutron Scattering and THz Spectroscopy* (Morgan & Claypool Publishers, 2018).
- [8] S. Toth, B. Lake, *J. Phys.: Condens. Matter* **27**, 166002 (2015).
- [9] Y. Zhou, K. Kanoda, T.-K. Ng, *Rev. Mod. Phys.* **89**, 025003 (2017).
- [10] I. A. Blech, B. L. Averbach, *Physics* **1**, 31 (1964).
- [11] D. Hohlwein, J.-U. Hoffmann, R. Schneider, *Phys. Rev. B* **68**, 140408 (2003).
- [12] S. T. Bramwell, *et al.*, *Phys. Rev. Lett.* **87**, 047205 (2001).
- [13] T. Fennell, *et al.*, *Science* **326**, 415 (2009).
- [14] T. Yavors’kii, T. Fennell, M. J. P. Gingras, S. T. Bramwell, *Phys. Rev. Lett.* **101**, 037204 (2008).
- [15] R. Sibille, *et al.*, *Nat. Phys.* **14**, 711 (2018).
- [16] J. A. M. Paddison, *et al.*, *Phys. Rev. Lett.* **110**, 267207 (2013).
- [17] J. A. M. Paddison, *et al.*, *Nat. Phys.* **13**, 117 (2017).
- [18] X. Bai, *et al.*, *Phys. Rev. Lett.* **122**, 097201 (2019).
- [19] Y. Li, *et al.*, *Nat. Commun.* **8**, 15814 (2017).
- [20] S. Gao, *et al.*, *Nat. Phys.* **13**, 157 (2017).
- [21] S. Chillal, *et al.*, *Nat. Commun.* **11**, 2348 (2020).
- [22] S. Gao, *et al.*, *Nature* **586**, 37 (2020).
- [23] J. A. M. Paddison, *et al.*, *Phys. Rev. Lett.* **129**, 137202 (2022).
- [24] J. A. M. Paddison, *Phys. Rev. Lett.* **125**, 247202 (2020).
- [25] A. Kitaev, *Ann. Phys.* **303**, 2 (2003).
- [26] M. G. Tucker, D. A. Keen, M. T. Dove, A. L. Goodwin, Q. Hui, *J. Phys.: Condens. Matter* **19**, 335218 (2007).
- [27] A. Mellergård, R. L. McGreevy, A. Wannberg, B. Trostell, *J. Phys.: Condens. Matter* **10**, 9401 (1998).
- [28] J. A. M. Paddison, J. R. Stewart, A. L. Goodwin, *J. Phys.: Condens. Matter* **25**, 454220 (2013).
- [29] D. R. Harcombe, P. G. Welch, P. Manuel, P. J. Saines, A. L. Goodwin, *Phys. Rev. B* **94**, 174429 (2016).
- [30] M. A. McGuire, V. O. Garlea, *Phys. Rev. B* **93**, 054404 (2016).
- [31] G. J. Nilsen, C. M. Thompson, G. Ehlers, C. A. Marjerrison, J. E. Greedan, *Phys. Rev. B* **91**, 054415 (2015).
- [32] J. A. M. Paddison, *et al.*, *Phys. Rev. B* **97**, 014429 (2018).
- [33] Z. J. Morgan, H. D. Zhou, B. C. Chakoumakos, F. Ye, *J. Appl. Crystallogr.* **54**, 1867 (2021).
- [34] B. A. Frandsen, X. Yang, S. J. L. Billinge, *Acta Crystallogr. A* **70**, 3 (2014).
- [35] B. A. Frandsen, S. J. L. Billinge, *Acta Crystallogr. A* **71**, 325 (2015).
- [36] H. L. Andersen, *et al.*, *IUCrJ* **8**, 33 (2021).
- [37] R. Baral, *et al.*, *Matter* **5**, 1853 (2022).
- [38] B. A. Frandsen, P. K. Hamilton, J. A. Christensen, E. Stubben, S. J. L. Billinge, *J. Appl. Crystallogr.* **55** (2022).
- [39] J. A. M. Paddison, *et al.*, *Nat. Commun.* **7**, 13842 (2016).
- [40] W. Kinney, W. Wolf, *J. Appl. Phys.* **50**, 2115 (1979).
- [41] P. Schiffer, *et al.*, *Phys. Rev. Lett.* **74**, 2379 (1995).
- [42] O. A. Petrenko, C. Ritter, M. Yethiraj, D. McK Paul, *Phys. Rev. Lett.* **80**, 4570 (1998).
- [43] T. Yavors’kii, M. Enjalran, M. J. P. Gingras, *Phys. Rev. Lett.* **97**, 267203 (2006).
- [44] J. A. M. Paddison, *et al.*, *Science* **350**, 179 (2015).
- [45] N. d’Ambrumenil, O. A. Petrenko, H. Mutka, P. P. Deen, *Phys. Rev. Lett.* **114**, 227203 (2015).
- [46] M. Enjalran, M. J. P. Gingras, *Phys. Rev. B* **70**, 174426 (2004).
- [47] N. Qureshi, *J. Appl. Crystallogr.* **52**, 175 (2019).
- [48] R. Brout, H. Thomas, *Physica Physique Fizika* **3**, 317 (1967).
- [49] D. E. Logan, Y. H. Szczech, M. A. Tusch, *Europhys. Lett. (EPL)* **30**, 307 (1995).
- [50] M. P. Eastwood, D. E. Logan, *Phys. Rev. B* **52**, 9455 (1995).
- [51] G. M. Wysin, *Phys. Rev. B* **62**, 3251 (2000).
- [52] C. Scherer, I. Aveline, *physica status solidi (b)* **75**, 465 (1976).
- [53] C. Scherer, Y. Barjhoux, *physica status solidi (b)* **80**, 313 (1977).
- [54] P. H. Conlon, J. T. Chalker, *Phys. Rev. B* **81**, 224413 (2010).
- [55] S. W. Lovesey, *Theory of Neutron Scattering from Condensed Matter: Polarization Effects and Magnetic Scattering*, vol. 2 (Oxford University Press, Oxford, 1987).
- [56] P. J. Brown, *International Tables for Crystallography* (Kluwer Academic Publishers, Dordrecht, 2004), vol. C, chap. Magnetic Form Factors, pp. 454–460.
- [57] J. N. Reimers, A. J. Berlinsky, A.-C. Shi, *Phys. Rev. B* **43**, 865 (1991).
- [58] B. Canals, C. Lacroix, *Phys. Rev. B* **61**, 11251 (2000).
- [59] V. I. Lebedev, D. Laikov, *Doklady Mathematics* (Pleiades Publishing, Ltd., 1999), vol. 59, pp. 477–481.
- [60] S. Mugiraneza, A. M. Hallas, *Commun. Phys.* **5**, 95 (2022).
- [61] K. W. Plumb, *et al.*, *Nat. Phys.* **15**, 54 (2019).
- [62] A. Pires, D. Hone, *J. Phys. Soc. Jpn.* **44**, 43 (1978).
- [63] T. Proffen, T. R. Welberry, *Acta Crystallogr. A* **53**, 202 (1997).
- [64] F. James, M. Roos, *Comp. Phys. Commun.* **10**, 343 (1975).
- [65] F. James, *MINUIT Function Minimization and Error Analysis: Reference Manual Version 94.1*, CERN (1994).
- [66] C. G. Shull, J. S. Smart, *Phys. Rev.* **76**, 1256 (1949).
- [67] G. Pokharel, *et al.*, *Phys. Rev. Lett.* **125**, 167201 (2020).
- [68] P. G. Welch, *et al.*, *Phys. Rev. B* **105**, 094402 (2022).
- [69] H. Ikeda, M. T. Hutchings, *Journal of Physics C: Solid State Physics* **11**, L529 (1978).
- [70] D. Dahlbom, C. Miles, H. Zhang, C. D. Batista, K. Barros, *arXiv 2209.01265* (2022).
- [71] Y.-L. Wang, B. R. Cooper, *Phys. Rev.* **172**, 539 (1968).
- [72] V. H. Santos, C. Scherer, *Z. Phys. B* **40**, 95 (1980).
- [73] A. O. Scheie, *et al.*, *arXiv 2109.11527* (2021).
- [74] A. O. Scheie, *et al.*, *arXiv 2207.14785* (2022).